한국박용기관학회지 제28권, 제5호, pp. 717~727, 2004. 7 (ISSN 1226-9549)
Journal of the Korean Society of Marine Engineers

차분래티스 볼츠만 법을 이용한 저Mach수 흐름에서의 유동소음해석

강호근† · 김은라* · 김정환**

(원고접수일 : 2004년 1월 29일, 심사완료일 : 2004년 5월 24일)

Numerical Simulation of Aeroacoustic Noise at Low Mach Number Flows by Using the Finite Difference Lattice Boltzmann Method

Ho-Keun Kang† · Eun-Ra Kim* · Jeong-Hwan Kim**

Abstract : In this study, we simulate the aerodynamic sounds generated by a two-dimensional circular cylinder in a uniform flow are simulated by applying the finite difference lattice Boltzmann method (FDLBM). The third-order-accurate up-wind scheme (UTOPIA) is used for the spatial derivatives, and the second-order-accurate Runge-Kutta scheme is applied for the time marching. The results show that we successively capture very small acoustic pressure fluctuations with the same frequency of the Karman vortex street compared with the pressure fluctuation around a circular cylinder. The propagation velocity of the acoustic waves shows that the points of peak pressure are biased upstream due to the Doppler effect in the uniform flow. For the downstream, on the other hand, it quickly propagates. It is also apparent that the amplitude of sound pressure is proportional to $r^{-1/2}$, r being the distance from the center of the circular cylinder.

To investigate the effect of the lattice dependence, furthermore, a 2D computation of the tone noise radiated by a NACA0012 with a blunt trailing edge at high incidence and low Reynolds number is also investigated.

Key words : Aeroacoustic, Aeolian Tones, Lattice Boltzmann Method, Mach Number

1. Introduction

In recent years, works in the field of computational aeroacoustics (CAA) have much been progressed via direct simulation by using a large amount of computer resources.

Within the CAA field, several different approaches have been developed. The first group, referred to as a hybrid

† 책임저자(경상대학교 기계항공공학부 · 해양산업연구소), E-mail : kang88@gaechuk.gsnu.ac.kr, T : 055)640-3064
* 전북대학교 공업기술연구센터 연구원
** 한국조선기자재연구원 선임연구원

method, makes use of an acoustic analogy, under the assumption of a compact source, to predict the far-field sound[1],[2]. The source terms are evaluated using the near-field flow quantities, which are obtained by solving the incompressible Navier-Stokes equations for low Mach number flows. This method saves computational time as well as memory storage compared with DNS, because the flow in the far-field is assumed to be stationary or uniform and thus not solved numerically. The second group of approaches, often called the acoustic/viscous splitting method, assumes that flow quantities are represented, under the assumption of low Mach number, by an incompressible mean flow and a perturbation about the mean [3]-[5]. In the far field, the perturbation quantities are equivalent to acoustic quantities. This method may possibly be a convenient method of predicting sound field resulting from low Mach number, non-compact source region. So far the results obtained by this method are qualitative, and detailed description of sound field have not yet been given. The third group makes use of DNS, where both the fluid motion and the sound which it generates are directly computed [6],[7]. Recent development of a high-performance supercomputer and highly-accurate numerical schemes makes it possible to simulate a sound field by directly solving the compressible Navier-Stokes equations over the entire region from near to far fields. This method does not suffer from restrictions such as low Mach number and compactness of the source region, but requires a large amount of computer resources. So far most of the computational work on the sound generation due to flow past a circular cylinder has been done using the above stated method, but the studies using lattice Boltzmann method (LBM) or finite difference lattice Boltzmann method (FDLBM) are very few.

In the present study, using FDLBM over the entire region from the near to far fields, the generation and propagation mechanism of the acoustic waves produced by a turbulent wake of a circular cylinder in a uniform flow at low Reynolds number is computed. The predicted sound spectra with the vortex/flow dynamics is clarified and the effect of the Mach number using the sound velocity is also examined. In order to see the characteristic of the lattice dependence, besides, a 2-dimensional computation of the tone noise radiated by a NACA0012 with a blunt trailing edge at high incidence and low Reynolds number is also investigated.

2. Mathematical Formulation

Lattice Boltzmann simulations [8]-[10] solve the Navier-Stokes equations by following the evolution of a set of distribution functions, $f_i(x, t)$, which represent the density at time t and lattice site x which is travelling with velocity c_i. The velocity vectors c_i are such that the distribution functions advect to neighbouring lattice sites $x+\triangle x$ in the time interval $\triangle t$. Namely,

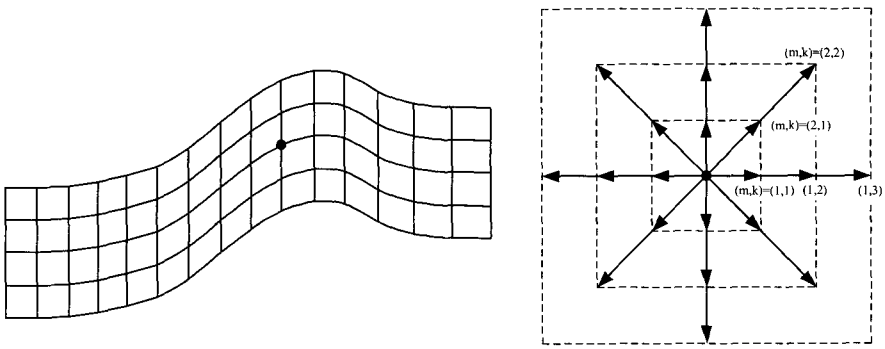

Fig. 1 Grid system in a body fitted curvilinear for a 2D21V model

the LBM solves the microscopic kinetic equation for particle distribution function from which the macroscopic quantities (velocity and density) are obtained through the movement and the collision of particles.

The presently popular method uses regularly spaced lattices and cannot handle curved boundaries with desirable flexibility. To circumvent such difficulties, the finite difference lattice Boltzmann method (FDLBM) [11],[12] in curvilinear coordinates is explored using body-fitted coordinates with non-uniform grids [13] as shown in Fig.1(a). Therefore, the FDLBM become possible and easy to simulate the complicated object shapes, and the application to various flow fields is attained.

2.1 Discretized Lattice BGK Model

The distribution function f_i are evolved according to a lattice Boltzmann equation assuming a single relaxation time approximation which Bhatnagar, Gross and Krook [14] first introduced in order to simplify the collision term.

$$\frac{\partial f_i}{\partial t} + \boldsymbol{c}_i \cdot \nabla f_i = -\frac{1}{\phi}(f_i - f_i^{eq}) \tag{1}$$

Here ϕ is the relaxation time and f_i^{eq} is the equilibrium distribution function of f_i at time step t, moving in direction i. The equilibrium distribution determines the physics inherent in the simulation. A power series in the local velocity is expressed as according to Kang et al.(2002) [15].

$$f_i^{eq} = F_i\rho\Big[1 - 2Bc_{i\alpha}u_\alpha + 2B^2(c_{i\alpha}u_\alpha) + Bu^2 - \frac{4}{3}B^3(c_{i\alpha}u_\alpha) - 2B^2 c_{i\alpha}u_\alpha u^2\Big] \tag{2}$$

In a 2D, 21-speed particle model (see Fig. 1(b)), the velocity of particles is determined by

$$c_i = k\sqrt{m}c\Big[\cos\Big(\frac{\pi(i-1)}{2} + \frac{\pi(i-1)}{4}\Big), \sin\Big(\frac{\pi(i-1)}{2} + \frac{\pi(i-1)}{4}\Big)\Big] \tag{3}$$
$$(i = 1, \cdots, 4,\ m = 1, 2,\ k = 1, 2, \cdots)$$

The index $m=1$ indicates the particle which moves in the orthogonal direction and $m=2$ indicates the particle which moves in the diagonal direction. The k

represents the speed of particle which moves in the nearest neighboring lattice. It is noted that Eq.(1) is one of numerous possible ways to model the transport of f_i. The density ρ, momentum flux $\rho\,\mathbf{u}$ and internal energy e are obtained from

$$\rho=\sum_i f_i,\quad \rho\,\mathbf{u}=\sum_i \mathbf{c}_i f_i \text{ and}$$

$$\rho e=\sum_i \frac{1}{2}c^2 f_i-\frac{1}{2}\rho u^2 \qquad (4)\text{-}(6)$$

2.2 Modifying Finite Difference Lattice Boltzmann Method

The models for compressible fluids are sometimes unstable in calculation. But by using the finite difference, it stabilizes the calculation considerably.

For this purpose, this study employs the discretized BGK equation (1). This equation is shown to lead the Navier-Stokes equations by the Chapmen-Enskog expansion, and the term $(\phi-1/2)$ in transfer coefficient changes into ϕ. The relationship between the kinematic viscosity and relaxation time factor becomes,

$$\mu=\frac{2}{D}\rho e\phi \qquad (7)$$

where D is the characteristic dimension and the value of D is 2 for two-dimensional cases. For high Reynolds number flows which are very important in engineering fields, $\mu\ll 1$ must be satisfied. If Euler's first order forward difference scheme is used for time integral, the equation is transformed as

$$f_i^{n+1}=f_i^n+\Delta t\left[-c_{i\alpha}\frac{\partial f_i^n}{\partial x_\alpha}-\frac{1}{\phi}(f_i^n-f_i^{eq})\right] \qquad (8)$$

where Δt is the time increment. In Eq. (8), the condition of stability for the collision term must be satisfied $\Delta t/\phi<2.0$, which states that the distribution function approaches its equilibrium state by every collision. Relations between μ and $\Delta t/\phi$ lead that, for high Reynolds

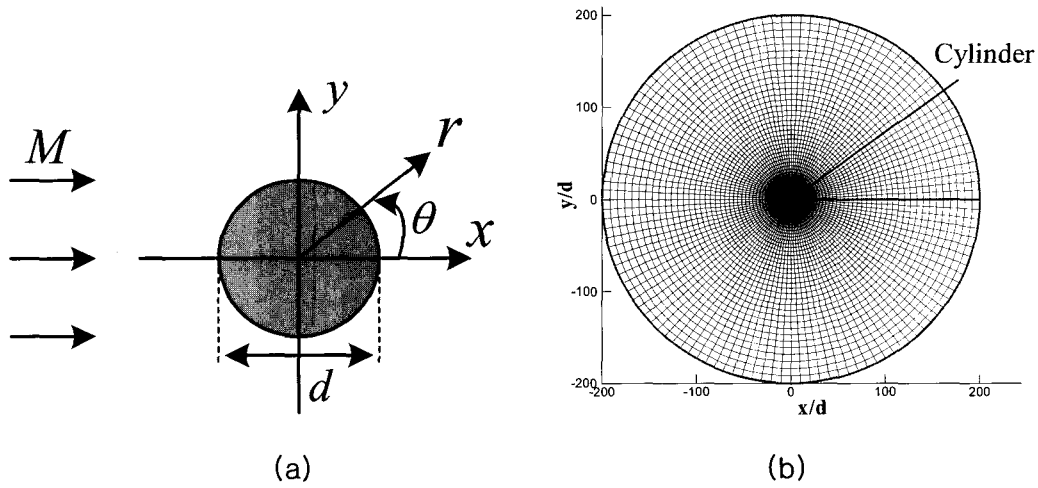

Fig. 2 Schematic diagram of the flow field (a) and computational mesh for flow past a circular cylinder (b). For clarity, only one in every four mesh lines for the radial direction is plotted.

number flows, the time increment chosen must be very small and the calculation time will be very long.

Therefore, an equation in which the third term is added to the discretized BGK equation (Eq. (1)) is transformed

$$\frac{\partial f_i}{\partial t}+c_{i\alpha}\frac{\partial f_i}{\partial x_\alpha}-\frac{Ac_{i\alpha}}{\phi}\frac{\partial}{\partial x_\alpha}(f_i-f_i^{eq}) =-\frac{1}{\phi}(f_i-f_i^{eq}) \tag{9}$$

where $A(>0)$ is a constant. Then the relationship is changed as follows.

$$\mu=\frac{2}{D}\rho e(\phi-A) \tag{10}$$

By conducting such conversion, it is possible to modify the relationship between the coefficient of the kinematic viscosity and the single relaxation coefficient $\phi\sim\mu$ to $\phi-A\sim\mu$ in FDLBM. Therefore, the single relaxation coefficient ϕ becomes $\phi\rightarrow A$ in the flow of high Reynolds number, and the transformed model of FDLBM makes it possible to calculate with the fixed value of ϕ which is taken in high Reynolds number flows. Also, it becomes possible that the calculation of Δt can easily or stably simulate up to large value, while $\Delta t/\phi=2.0$ is an upper limit for the collision term in the conventional FDLBM model.

3. Numerical Method

A schematic diagram of the flow model is presented in Fig. 2(a). In the Cartesian coordinate (x, y), the uniform flow of the velocity U_0 parallel to the x direction is considered. Normalized by the static sound velocity a_0, the streamwise velocity is prescribed by the $M=U_0/a_0=U_0/\sqrt{2e}$, where M is the Mach number. Furthermore, the cylinder of the diameter d is fixed at the origin. The polar coordinates (r, θ) are also used, where the azimuthal angle θ is defined from downstream in the counterclockwise direction. The Reynolds number, defined as $Re=U_0d/\nu$, where ν is the kinematic viscosity, is equal to 150. Flow quantities are non-dimensionalized by d, a_0, and ρ_0, where ρ_0 is the ambient density. The physical parameter prescribed is the ratio of specific heats $\gamma=(D+2)/D$.

For the entire field from near to far acoustic field, computations are carried out on a O-grid configuration shown in Fig. 2(b), where only one-quarter of the mesh lines for the radial direction are plotted for clarity. A typical grid system in the case of $Re=150$ is constructed as follows: the number of the grid points results in $r\times\theta=201$ (in the radial direction) $\times 121$ (in the azimuthal direction); the time increment Δt is 0.02; and the examined Mach numbers use the sound velocity by changing the internal energy e. All the calculations are in two-dimension and use 2D21V model. Computations start with uniform velocity $u_i(t=0)=(U_0, 0)$ everywhere.

For spatial derivatives, a third-order-accurate up-wind scheme (second-order-accurate at the boundary) is used, and a second-order-accurate Runge-Kutta scheme is used for time integration. Adiabatic and no-slip conditions are adopted on the

cylinder surface, and the detailed boundary condition at the solid wall is presented by Kang and Kim[16]. Along the O-grid shaped outer boundary, the velocities are set at the free stream values, $u_i=(U_0,0)$. Because the boundary is sufficiently far away from the circular cylinder, the numerical wave reflections from the boundary are removed [17]. The spacing in the surface region is prescribed to be fine enough to analyze the boundary layer on the cylinder surface. The acquired data is set forth sufficiently after the effect of the initial perturbation become negligible ($t\geq 100$).

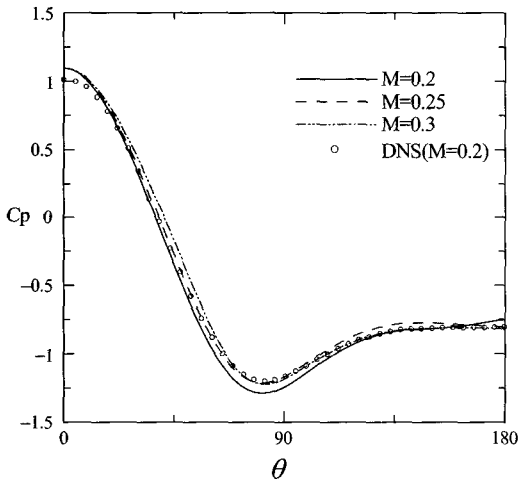

Fig. 3 Time averaged pressure Cp at M=0.2, 0.25, 0.3 and DNS result (Inoue, 2002)

Furthermore, to validate the lattice dependence, we consider the unsteady flowfield and the sound generated by a NACA0012 airfoil placed in a two-dimensional uniform flow. The airfoil angle of attack is $\alpha=14$ deg. All calculation conditions are the same in case of the circular cylinder.

4. Results and Discussion

4.1 Aeolian tone

A flow past a circular cylinder at $M=0.2$ and $Re=150$ is considered for validation of the modified FDLB model (Eq. (9)), in which the cylindrical coordinated system is applied. The calculation results when the Karman vortex street was fully developed are shown in Figs. 3 to 8.

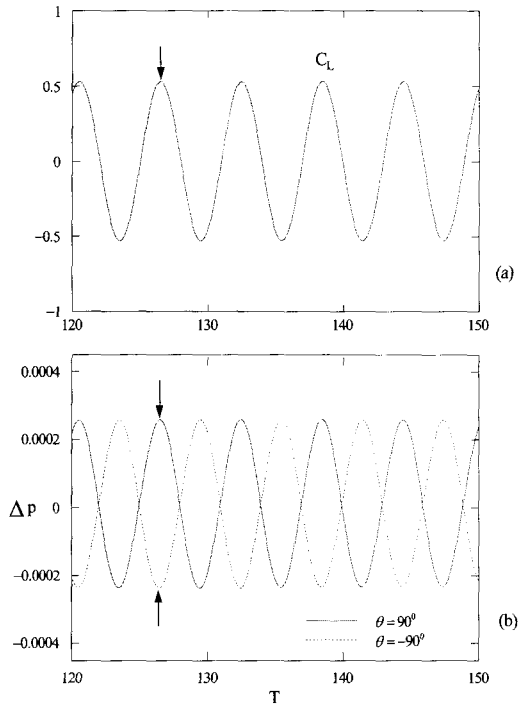

Fig. 4 Lift force acting on the cylinder surface (a) and time history of the sound pressure (b). M=0.2, Re=150. Arrows indicates T=127. d=50; red line $\theta=90^0$; blue line $\theta=-90^0$.

Force acting on the cylinder surface as a function of the azimuthal angle θ is presented in Fig. 3 for three different Mach number ($M=0.2$, 0.25 and 0.3), and

compared with that of DNS [7]. Pressure coefficient C_p is the time averaged pressure on the cylinder surface normalized by the value at the stagnation point $\theta=0^0$. It shows that the coefficient C_p is not affected significantly by the Mach number. A comparison of the pressure coefficient at $0\leq\theta\leq\pi$ for $M=0.2$ also indicates that FDLBM is compatible with DNS.

In order to observe the near-field flow structure, lift force acting on the cylinder surface and pressure variations are plotted in Fig. 4 for the case of $M=0.2$ ($e=0.5$). Here, the sound pressure Δp is defined as

$$\Delta p=\frac{p-p_0}{p_0}=\frac{p-\rho_0 e_0}{\rho_0 e_0} \tag{11}$$

where p_0 denotes the ambient pressure. Time history of sound pressure at the point $d=50$ and $\theta=90^0$ and -90^0 is shown in Fig. 4(b). By comparing with the lift coefficient C_L in Fig. 4(a), during the period $T(=Ut/d)=120-150$, it can be seen that the period of C_L oscillates equal to the period of Δp.

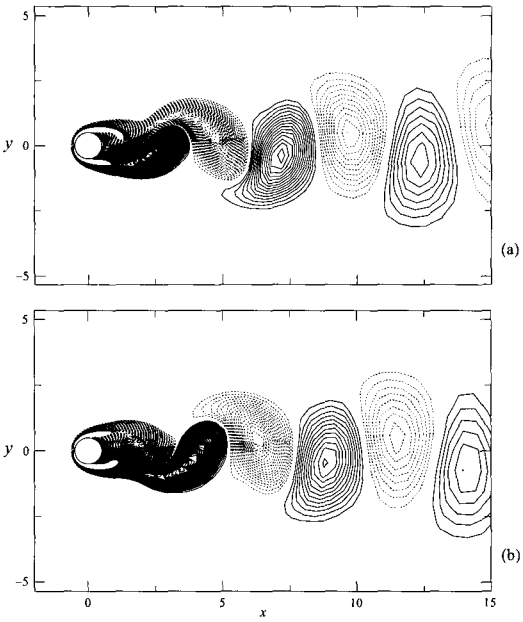

Fig. 5 Vorticity contours at two different instants. M=0.2, Re=150. (a) T=127. (b) T=132

Positive peaks of C_L coincide with the positive and negative peaks of $\Delta p_{\theta=+90}$. In this case, the Strouhal number is defined by $S_t=fd/U$ where f is the frequency of the periodic vortex shedding. It is evaluated as $S_t=0.177$, which is very

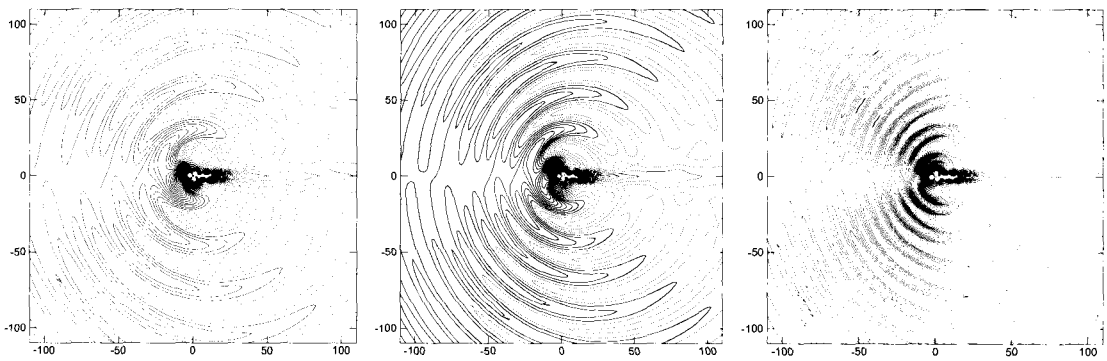

(a) M=0.2 (b) M=0.25 (c) M=0.3

Fig. 6 Contours of sound pressure at three different Mach numbers. T=132. Re=150. Solid lines: positive, dotted: negative

close to the experimental and DNS results for Re=150 [7]. The vorticity field in Fig. 5 shows that a vortex is shed from the upper side of the circular cylinder during the period (T=127 and 132) and, behind the cylinder, vortices become weaker with increasing downstream distance.

Figure 6 shows the acoustic pressure field at T=132 for three different Mach numbers (M=0.2, 0.25 and 0.3), where the contour level fluctuates at $\Delta p_{step}=3\times10^{-4}$, 7.5×10^{-3} and 1.0×10^{-3}, respectively. The solid lines indicate the positive pressures and the dashed lines are the negative ones. As can be seen from this figure, rarefaction waves with negative Δp and compression waves with positive Δp are generated alternately around the cylinder at the origin, and propagate downstream and upstream, respectively.

Figure 7 illustrates distributions and decays of the acoustic pressure waves

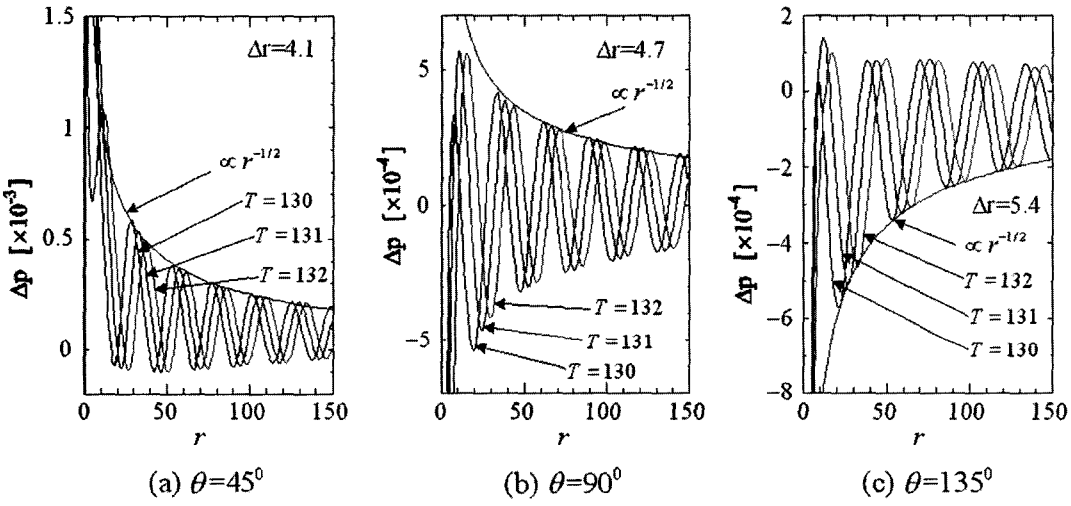

Fig. 7 Distributions and decays of sound pressure at the three different directions. Re=150, M=0.2.

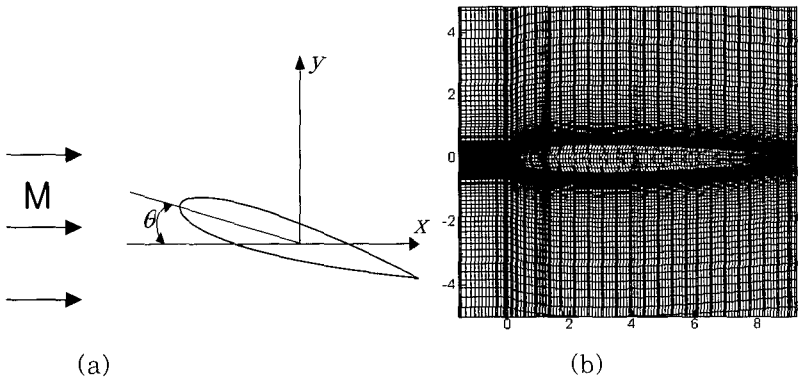

Fig. 8 Schematic diagram of the flow field (a) and computational mesh with NACA0012 (b).

plotted along the different directions ($\theta=45^0$, 90^0 and 135^0). The distribution of Δp are plotted against the radial distance r from the origin at the three different times $T=130$, 131, and 132, respectively. Each peak of the waves is found to propagate and decay. The propagation speed of the waves is equal to the speed of sound in the far field, in agreement with the linear acoustic theory. Also, the decaying curves are converged to the lines proportional to $r^{-1/2}$ in the far field, which is again in accordance with the theory.

4.2 Lattice dependence

The simulated flowfield around the airfoil for $M=0.2$ and $Re=200$ is presented in Fig. 8. No-slip velocity conditions are imposed on the airfoil surface. Figures 9 and 10 plot contour of the acoustic pressure and vorticity past a NACA0012 airfoil at 14 deg angle of attack, at a given time $T=156$, respectively. In this case the vortex shedding process, initiated by the instability of the separated upper shear layer near the midchord, is presented and the waves are seen to propagate from the airfoil along the normal direction of the flow. Therefore, the acoustic waves have an isotropic characteristic regardless of a lattice shape. In figure 10, it interacts with the lower boundary layer near the

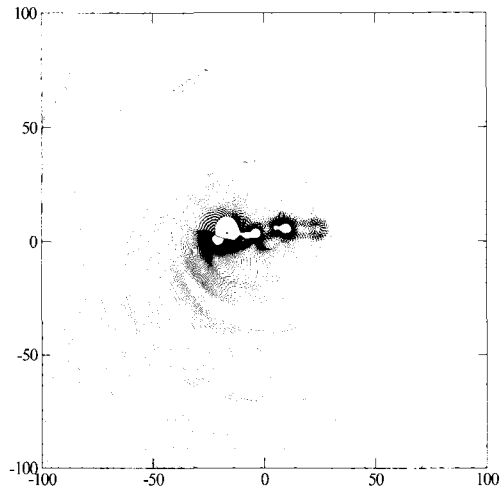

Fig. 9 Contours of sound pressure past a NACA0012 airfoil at 14 deg angle of attack. T=156, Re=200 and M=0.2.

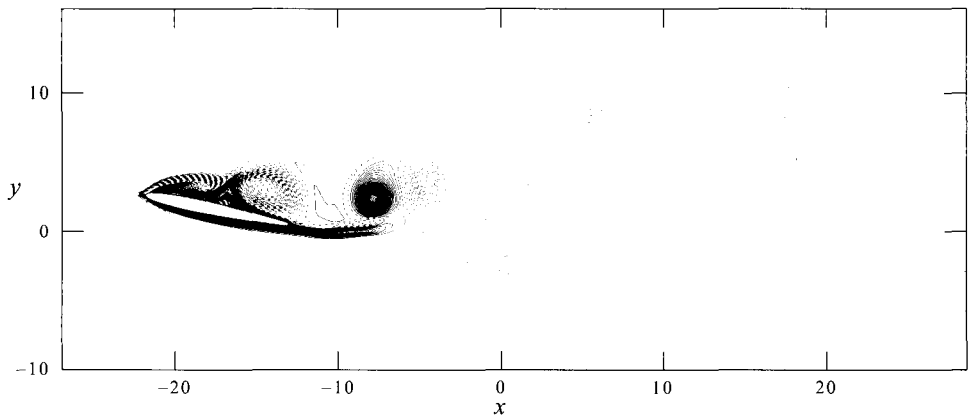

Fig. 10 Vorticity contours for a two-dimensional flow past a NACA0012 airfoil at 14 deg angle of attack. T=156. Re=200.

trailing edge to develop a periodic vortex shedding pattern. However, the unsteady flowfield and the sound generated by the NACA0012 airfoil should be studied more precisely in the future.

5. Concluding Remarks

The acoustic waves generated from the flow around a circular cylinder are successfully simulated using the FDLBM of the two-dimensional 21 velocity model. The sound frequency is the same as the vortex shedding frequency of the Karman vortex street. The rarefaction waves and the compression waves are alternately generated and propagate toward downstream and upstream, respectively. The sound pressure also decays proportional to $r^{-1/2}$ in the far acoustic field, which agrees with the theoretical prediction. These results suggest that the sounds generated from the cylinder at low Reynolds numbers are precisely captured by FDLBM if both the flow dynamics in the near field and the wave propagations in the far field are computed with high accuracy.

The finite difference based lattice Boltzmann method is shown to be a cost-effective method for computing sound generation and propagation for a wide range of flows.

References

[1] J. C. Hardin and S. L. Lamkin, "Aeroacoustic Computation of Cylinder Wake Flow", AIAA Journal, Vol. 22, pp. 51-57, 1984.

[2] J. S. Cox, K. S. Brentner and C. L. Rumsey, "Computation of Vortex Shedding and Radiated Sound for a Circular Cylinder: Subcritical to Transonic Reynolds Numbers", Theoret. Comput. Fluid Dyn.,, Vol. 12, pp. 233-253, 1998.

[3] J. C. Hardin and D. S. Pope, "An Acoustic/Viscous Splitting Technique for Computational Aeroacoustics", Theoret. Comput. Fluid Dyn.,, Vol. 6, pp. 323-340, 1994.

[4] W. Z. Shen and J. N. Sorensen, "Comment on the Aeroacoustic Formulation of Hardin and Pope", AIAA Journal, Vol. 37, pp. 141-143, 1999.

[5] S. A. Slimon, M. C. Soteriou and D. W. Davis, "Computational Aeroacoustic Simulation using the Expansion about Incompressible Flow Approach", AIAA Journal, Vol. 37, pp. 409-416, 1999.

[6] T. Colonius, S. K. Lele and P. Moin, "Sound Generation in a Mixing Layer", J. Fluid Mech., Vol. 330, pp. 375-409, 1997.

[7] O. Inoue and N. Hatakeyama, "Sound Generation by a two-dimensional Circular Cylinder in a Uniform Flow", J. Fluid Mech., Vol. 471, pp. 285-314, 2002.

[8] S. Chen and G. D. Doolen, "Lattice Boltzmann Method for Fluid Flows", An. Rev. Fluid Mech., Vol. 30, pp. 329-364, 1998.

[9] S. Succi, "The Lattice Boltzmann Equation: For Fluids and Beyond", Oxford University Press, 2001.

[10] M. R. Swift, E. Orlandini, W. R.

Osborn and J. M. Yeomans, "Lattice Boltzmann Simulations of Liquid-gas and Binary Fluid Systems", Phys. Rev., E 54, pp. 5041-5052, 1996.

[11] N. Cao, S. Chen, S. Jin and D. Martinez, "Physical Symmetry and Lattice Symmetry in the Lattice Boltzmann Method", Rhys. Rev. E, Vol. 55, pp. R21-R24, 1997.

[12] T. Seta, K. Kono, D. Martinez and S. Chen, "Lattice Boltzmann Scheme for Simulating Two-Phase Flows", Trans. JSME Journal, B, 65-634, pp. 1955-1963, 1999.

[13] R. Mei and W. Shyy, "On the Finite Difference-based Lattice Boltzmann Method in Curvilinear Coordinates", J. Comput. Phys., Vol. 143, pp. 426-448, 1998.

[14] P. L. Bhatnagar, E. P. Gross and M. Krook, "A Model for Collision Processes in Gases. I. Small Amplitude Processes in Charged and Neutral One-component Systems", Phys. Rev. 94(3), pp. 511-525, 1954.

[15] H. K. Kang, M. Tsutahara, K. D. Ro and Y. H. Lee, "Numerical Simulation of Shock Wave Propagation Using the Finite Difference Lattice Boltzmann Method", KSME Int. J, Vol. 16, No. 10, pp. 1327-1335, 2002.

[16] H. K. Kang and E. R. Kim, "Numerical Simulation of Aerodynamic Sound by the Finite Difference Lattice Boltzmann Method", J. of Ocean Engineering and Technology., Vol. 18, No. 2, pp. 10-17, 2004.

[17] T. Pointsot and S. K. Lele, "Boundary Conditions for Direct Simulation of Compressible Viscous Flows", J. Comput. Phys., Vol. 101, pp. 104-129, 1992.

저 자 소 개

강호근 (姜鎬根)

1969년 11월생. 1992년 한국해양대학교 기관공학과 졸업(학사). 1997년 한국해양대학교 기관공학과 졸업(석사). 2001년 Kobe Univ. 대학원 기계공학과 졸업(박사). 현재 경상대학교 기계항공공학부 BK교수

김은라 (金銀羅)

1973년생. 1995년 2월 전북대학교 지질학과 졸업. 2000년 2월 전북대학교 대학원 토목공학과 졸업(석사). 2003년 3월 Kobe Univ. 토목공학과 졸업(박사). 현재 전북대학교 공업기술연구센터 연구원.

김정환 (金貞奐)

1968년 2월생, 1998년 부경대학교 기계공학과 졸업(공학사), 2000년 부경대학교 대학원 기계공학과 졸업(공학석사), 2002년~2003년 일본큐슈공업대학 기계시스템공학과 특별연구생(일본학술진흥재단 지원), 2003년 8월 한국해양대학교 대학원 기계공학과 졸업(공학박사), 현재 한국조선기자재연구원 선임연구원.